Signal Processing 134 (2017) 185–196

Contents lists available at ScienceDirect

Signal Processing

journal homepage: www.elsevier.com/locate/sigpro

On the theory of function-valued mappings and its application to the processing of hyperspectral images

Daniel Otero[a], Davide La Torre[b,c], Oleg Michailovich[d], Edward R. Vrscay[a,*]

[a] Department of Applied Mathematics, University of Waterloo, ON, Canada
[b] Department of Economics, Management, and Quantitative Methods, University of Milan, Milan, Italy
[c] Department of Mathematics, Nazarbayev University, Astana, Kazakhstan
[d] Department of Electrical and Computer Engineering, University of Waterloo, ON, Canada

ARTICLE INFO

Keywords:
Function-valued functions
Image processing
Banach spaces
Fourier transform
And fractal transform

ABSTRACT

The concept of a mapping, which takes its values in an infinite-dimensional functional space, has been studied by the mathematical community since the third decade of the last century. This effort has produced a range of important contributions, many of which have already made their way to applied sciences, where they have been successfully used to facilitate numerous practical applications across various fields. Surprisingly enough, one particular field, which could have benefited from the above contributions to a much greater extent, still relies on finite-dimensional models and approximations, thus missing out on numerous advantages offered through adopting a more general framework. This field is image processing, which is in the focus of this study. In particular, in this paper, we introduce an alternative approach to the analysis of multidimensional imagery data based on the mathematical theory of function-valued mappings. In addition to extending various tools of standard functional calculus, we generalize the notions of Fourier and fractal transforms, followed by their application to processing of multispectral imaging data. Some applications and future extensions of this work are discussed as well.

1. Introduction

In imaging science, the concept of function-valued mappings generalizes the concept of vector-valued functions (or, equivalently, vector fields), the simplest example of which would be colour images [24]. In a more general case, vector-valued functions provide a quite natural, if not obvious, representation: associated with each pixel location x is an N-dimensional vector $u(x) = (u_1(x), u_2(x), \ldots, u_N(x)) \in \mathbb{R}^N$ of image values. Thus, in the context of hyperspectral imaging, $u(x)$ corresponds to N values of spectral reflectance, measured at the location x over N different wavelengths $\lambda_1, \lambda_2, \ldots, \lambda_N$. It is important to note, however, that the entries of $u(x)$ are, in fact, a discretization or sampling of the continuously defined spectral function at x.

As is well known, many image processing procedures performed on colour images (such as, for example, image compression) rely on colour-space transformations, intended to exploit the significant correlations between colour channels. Analogous procedures have been devised for higher-dimensional vector-valued images as well. Thus, for instance, it is common to reduce the correlation between different channels of hyperspectral images by means of principal component analysis (PCA), as discussed in [13]. In all such cases, the images thus obtained are consequently dealt with as "image cubes", in which case the range (e.g., $\mathbb{R}^N$) is simply regarded as an additional (discrete) coordinate.

As opposed to the "image cube" formalism, a number of very effective image processing solutions, capable of working directly on the correlated channels of vector-valued images, have been recently developed [21,7,22]. Rather than treating the range of such images as "yet another dimension", such methods are essentially vector-based, in the sense that they consider the input to be a *mapping* from its domain to $\mathbb{R}^N$. Naturally, this approach leads to an important question, namely: Could vector-valued images be better understood, and perhaps better algorithms be developed, if their range were a space of *continuously defined functions* instead of $\mathbb{R}^N$? To establish a "backward compatibility" between the continuous and discrete formulations, we recall an obvious fact: the elements of $\mathbb{R}^N$ admit an alternative interpretation as functions from $\{1, 2, \ldots, N\}$ to $\mathbb{R}$. Besides, the field of mathematical imaging has witnessed a great number of conceptual breakthroughs, which resulted from working with continuous counter-

* Corresponding author.
E-mail addresses: dotero@uwaterloo.ca (D. Otero), davide.latorre@unimi.it, davide.latorre@nu.edu.kz (D. La Torre), olegm@uwaterloo.ca (O. Michailovich), ervrscay@uwaterloo.ca (E.R. Vrscay).

http://dx.doi.org/10.1016/j.sigpro.2016.12.014
Received 22 April 2016; Received in revised form 16 October 2016; Accepted 12 December 2016
Available online 16 December 2016

parts of discrete images, viewed as elements of standard functional spaces, such as L^2. Should we not expect that the representation of, say, the spectral portions of hyperspectral images as functions could do the same?

To formalize the above conceptual generalization, we introduce an alternative representation of multivariate data as *function-valued mappings* (FVM) of the form,

$$u\colon X \to \mathcal{F}(Y), \tag{1}$$

where X denotes the support (aka domain) of the FVM, and $\mathcal{F}(Y)$ is a Banach space of either real- or complex-valued functions defined over an appropriate set Y. While X can still be a subset of either $\mathbb{R}^2$ or $\mathbb{R}^3$ (as it is usually the case with standard planar or volumetric images), the definition of $\mathcal{F}(Y)$ is problem-dependent. For example, in the case of hyperspectral images, we may consider $\mathcal{F}(Y) = L^2(\mathbb{R})$, which suggests that for each $x \in X$, the function $u(x) \in L^2(\mathbb{R})$ is a spectral function with finite energy. (That being said, it may be advantageous to consider functional spaces with much greater regularity, such as, e.g., the space of functions with bounded variation (BV) [11]. This is an open question that requires more study.)

At this point, it should be mentioned that outside of the area of imaging science, the FVM formalism has been widely used across different fields of mathematics, including partial differential equations [45], harmonic analysis [32,37], statistics [2], and analysis [16]. In fact, FVMs are known in the mathematical community as *Banach-valued functions* (BVF), studied by analysts who were mainly interested in extending the classical results of real-valued functions to a Banach-valued setting [16,10,14]. However, within the realm of applied sciences (and imaging sciences, in particular), the full potential of the FVM formalism remains largely untapped, apart from a few exceptions. For example, in [31], the authors use the FVM approach to analyze medical diagnostic data acquired by means of diffusion Magnetic Resonance Images (dMRI). An alternative to FVM was presented in [26] through the introduction of the concept of *measure*-valued functions/images, which have been shown to be well suited for *non-local* image processing. Indeed, non-local means (NLM) denoising [8,9] and fractal image coding [25] are only two among many image processing procedures which can be formulated and conceptualized using this measure-valued methodology, as demonstrated in [26].

We acknowledge that papers on remote sensing which employ "Banach space techniques" have appeared, e.g., [28,39]. The Banach spaces considered in these papers, however, involve the spatial domains of the hyperspectral images and not the spectral domains. Much closer to the spirit of function-valued mappings are papers which actually focus on the spectral functions comprising hyperspectral images, for example, dictionary methods [29] and basis expansions [12,36]. We also note the following paper which has emphasized the importance of determining proper spectral distance functions and metrics for hyperspectral image processing [15].

The main purpose of this paper is to set up a basic mathematical framework for FVMs. Based on this framework, we shall be able to extend the formulation of Fourier transform to FVMs, thereby paving the way for the extension of other standard transformations (such as, e.g., wavelet transform). We also consider a class of fractal transforms for FVMs, which have been used for the processing of hyperspectral images [42,43]. In particular, we demonstrate how a fractal transform on a FVM u induces a generalized fractal transform operator on the Fourier transform of u. It is hoped that our formulation of FVMs will stimulate further research, which could lead to new algorithms for the processing of multi-variable complex datasets, and of hyperspectral images, in particular.

2. Definition and motivation of FVMs

In what follows, we let X denote the domain of a FVM u, which is defined as a mathematical relation that assigns to every $x \in X$ a function f in some functional space $\mathcal{F}(Y)$, as suggested by (1). For the sake of concreteness, X and Y may be assumed to be sets in $\mathbb{R}^n$ and $\mathbb{R}^m$, respectively (unless stated otherwise). We also let the pairs $(X, \|\cdot\|_X)$ and $(\mathcal{F}(Y), \|\cdot\|_{\mathcal{F}(Y)})$ denote corresponding Banach spaces, with the elements of $\mathcal{F}(Y)$ being either real- or complex-valued functions supported on Y. Note that setting $X = \mathbb{R}^2$ and $\mathcal{F}(Y) = \mathbb{R}^n$ recovers the standard case of vector-valued functions/images, with hyperspectral imaging being among its most quintessential examples. As such, (1) can be considered to be a generalization of these classical representations.

Although in this paper we focus our attention on hyperspectral images, it is worthwhile to see how other kinds of data sets can be represented using the FVM approach.

Example 1. [31] dMRI is a powerful tool of modern medical imaging which allows a non-invasive probing of the diffusivity property of water molecules in vivo. In a particular variant of dMRI, known as high-angular resolution diffusion imaging (HARDI), the measurements are acquired at different anatomical locations over a range of orientations of diffusion encoding. Such signals may, therefore, be conveniently represented by a FVM $u\colon X \subset \mathbb{R}^3 \to \mathbb{L}^2(\mathbb{S}^2)$, where $\mathcal{F}(Y) = \mathbb{L}^2(\mathbb{S}^2)$ is the space of square-integrable functions supported on the unit sphere $\mathbb{S}^2$.

Example 2. A sensor network [41] may be considered as a FVM $u\colon X \to \mathcal{F}(Y)$, where X is a graph and $\mathcal{F}(Y)$ is, e.g., the space of square integrable functions that are supported on a subset of $\mathbb{R}$.

Example 3. A video sequence may be viewed as a FVM $u\colon X \subset \mathbb{R}^2 \to BV(Y)$, where $BV(Y)$ is the space of functions of bounded variation and Y is a subset of the real line. In a video, at each $x \in X$ we may have functions with discontinuities, and thus the function space $BV(Y)$ seems to be a reasonable choice for the range of u.

3. Mathematical foundation of FVMs

In this section, we present the mathematical foundation of FVM processing, which consists of three parts: (i) calculus of FVMs, (ii) L^P spaces of FVMs, and (iii) the Euler-Lagrange equation for FVM-based functionals. In each of the above cases, we introduce associated mathematical concepts that are employed throughout this paper. The reader who is familiar with the basic mathematical concepts of functions that take values in a Banach space may skip this section.

3.1. Calculus of FVMs

As with the calculus of real-valued functions, the concept of limit is also fundamental to the calculus of FVMs, which we introduce in the following definition.

Definition 1. Let $u\colon X \subset \mathbb{R}^n \to \mathcal{F}(Y)$. Let x_0 be a point that belongs to either X or its boundary ∂X, and let $\mathcal{N}$ be an open neighbourhood of $f \in \mathcal{F}(Y)$. We say that u is eventually in $\mathcal{N}$ as x approaches x_0 in the $\|\cdot\|_X$ sense if there exists an open neighbourhood $\mathcal{M}$ of x_0 such that $x \neq x_0$, $x \in \mathcal{M}$, and $x \in X$ implies that $u(x) \in \mathcal{N}$. We say that u tends to f when x tends to x_0, which we write as

$$\lim_{x \to x_0} u(x) = f,$$

when, for any neighbourhood $\mathcal{N}$ of f, u is eventually in $\mathcal{N}$ as x approaches x_0. If, as x tends to x_0, $u(x)$ does not approach any particular function $f \in \mathcal{F}(Y)$ in the $\|\cdot\|_{\mathcal{F}(Y)}$ sense, then we say that the limit of u as $x \to x_0$ does not exist.

The following theorem shows that Definition 1 has an ε-δ counterpart.

Theorem 1. *Let $u\colon X \subset \mathbb{R}^n \to \mathcal{F}(Y)$ and let x_0 be a point in either X or its boundary ∂X. Then $\lim_{x \to x_0} u(x) = f$ if and only if for all $\varepsilon > 0$ there exists $\delta > 0$ such that, for $x \in X$ that satisfies $0 < \| x - x_0 \|_X \leq \delta$, we*

have that $\| u(x) - f \|_{\mathcal{F}(Y)} \leq \varepsilon$.

Proof. See Theorem 3.1.1 of [34]. □.

As mentioned earlier, an FVM is a mapping between two Banach spaces. As such, the derivative of an FVM u at a given point $x_0 \in X \subset \mathbb{R}^n$ may be defined by means of the Fréchet derivative:

Definition 2. Let $u: X \subset \mathbb{R}^n \to \mathcal{F}(Y)$. We say that $Du(x_0)$ is the (Fréchet) derivative of u at $x_0 \in X$ if

$$\lim_{h \to 0} \frac{\| u(x_0 + h) - u(x_0) - Du(x_0)h \|_{\mathcal{F}(Y)}}{\| h \|_X} = 0. \tag{2}$$

Moreover, $Du: X \to \mathcal{F}(Y)$ is bounded and linear. Also, if (2) exists at all $x_0 \in X$, we say that u is differentiable in X in the $\|\cdot\|_{\mathcal{F}(Y)}$ sense.

As in the case of real-valued functions of several variables, FVMs also have a directional derivative. Such a derivative can be defined by means of the Gâteaux derivative.

Definition 3. Let $u: X \subset \mathbb{R}^n \to \mathcal{F}(Y)$. We say that $Du(x_0; h)$ is the directional derivative of u at $x_o \in X$ in the direction of $h \in \mathbb{R}^n$ if the limit

$$Du(x_0; h) = \lim_{\varepsilon \downarrow 0} \frac{u(x_0 + \varepsilon h) - u(x_0)}{\varepsilon} \tag{3}$$

exists. If (3) holds for all $x \in X$, we say that u is Gâteaux differentiable in X.As usual, Fréchet differentiability implies Gâteaux differentiability, while the opposite direction does not necessarily follow.

In the case of $X \subset \mathbb{R}^n$, we can define the partial derivatives of $u(x) = u(x_1, \ldots, x_n)$ with respect to the coordinates x_i. Specifically, as in the case of standard calculus, the partial derivative $\partial u/\partial x_i$ is defined as the following directional derivative,

$$\frac{\partial u}{\partial x_i} = \lim_{h \to 0} \frac{u(x_1, \ldots, x_i + h, \ldots, x_n) - u(x_1, \ldots, x_i, \ldots, x_n)}{h}. \tag{4}$$

Theorem 2. *If the partial derivatives* $\partial u/\partial x_i$ *exist at every* $x \in X$, *and if, for all* i, *the mappings* $\partial u/\partial x_i: X \subset \mathbb{R}^n \to \mathcal{F}(Y)$ *are continuous at a point* $x_0 \in X$, *then* u *is differentiable at* x_0.

Proof. See Proposition 3.7.2 of [10]. □.

Theorem 2 implies that, at each $x \in X$, $Du(x)$ can be considered to be a member of the product space $\mathfrak{F} := \mathcal{F}(Y) \times \mathcal{F}(Y) \times \cdots \times \mathcal{F}(Y) = \mathcal{F}(Y)^n$, and thus the derivative Du can be viewed as an operator from X to $\mathfrak{F}$, which can be shown to be bounded. In what follows, we denote this operator by ∇_{xu}.

The integration of FVMs can be defined by means of the *Bochner integral* [2,6], which is a natural generalization of the Lebesgue integral for mappings that take their values in a Banach space. The Bochner integral inherits many properties of Lebesgue integration, chief among which is linearity.

Definition 4. Let $u: X \subseteq \mathbb{R}^n \to \mathcal{F}(Y)$ and let (X, Σ, μ) be a measure space, where μ is the canonical Lebesgue measure and Σ is a σ-algebra of X. We say that u is measurable if there exists a sequence $\{\varphi_n\}$ of X-simple mappings, where $\varphi_n: X \subseteq \mathbb{R}^n \to \mathcal{F}(Y)$, such that $\lim_{n \to \infty} \| u(x) - \varphi_n(x) \|_{\mathcal{F}(Y)} = 0$ for almost all $x \in X$ in the sense of Lebesgue measure.

In the context of the above definition, an *X-step mapping* is a measurable mapping $\varphi: X \to \mathcal{F}(Y)$ with finite range: that is, φ is a mapping such that its range is the set

$$R(\varphi) = \{f_i : f_i \in \mathcal{F}(Y),\ i \in \mathbb{N},\ 1 \leq i \leq n\}, \tag{5}$$

and whose inverse mapping φ^{-1} assigns to every $f_i \in R(\varphi)$ its corresponding measurable set $A_i \in \Sigma$; i.e.,

$$A_i = \varphi^{-1}(f_i) \in \Sigma, \tag{6}$$

for all i, with $\mu(A_i) < \infty$ for every non-zero f_i. If the condition $\mu(A_i) < \infty$ is dropped, then φ is called an *X-simple mapping*. Both X-simple and X-step mappings can be represented in terms of the usual characteristic function χ as given by

$$\varphi(x) = \sum_{i=1}^{n} f_i \chi_{A_i}(x), \tag{7}$$

where, for a set D, $\chi_D(x) = 1$ if $x \in D$ and zero otherwise. In particular, the integral of an X-step mapping is given by

$$\int \varphi d\mu = \sum_{i=1}^{n} \mu(A_i) f_i. \tag{8}$$

Furthermore, the integral of φ over any $D \in \Sigma$ is defined as

$$\int_D \varphi d\mu = \int \varphi \chi_D d\mu. \tag{9}$$

Based on the above definition, we can now formally define the integral of a measurable FVM as follows.

Definition 5. Let $u: X \subseteq \mathbb{R}^n \to \mathcal{F}(Y)$. Also, let Σ be a σ-algebra of X and (X, Σ, μ) be a measure space endowed with the Lebesgue measure. If u is measurable, we say that u is integrable if there exists a sequence $\{\varphi_n\}$ of X-simple mappings such that the real-valued function $\| u(x) - \varphi_n(x) \|_{\mathcal{F}(Y)}$ is Lebesgue integrable for each n and

$$\lim_{n \to \infty} \int \| u(x) - \varphi_n(x) \|_{\mathcal{F}(Y)}\, dx = 0. \tag{10}$$

Moreover, for each $D \in \Sigma$, the integral of u over D is defined as

$$\int_D u(x) dx := \lim_{n \to \infty} \int_D \varphi_n(x) dx. \tag{11}$$

The latter definition of integrability might be difficult to apply in general. However, for finite measure spaces, the integrability of a measurable FVM is easier to verify based on the following criterion.

Theorem 3. *Let* $u: X \subseteq \mathbb{R}^n \to \mathcal{F}(Y)$ *be a measurable* FVM, *and let* (X, Σ, μ) *be a finite measure space. Then,* u *is integrable if and only if* $\| u(x) \|_{\mathcal{F}(Y)}$ *is Lebesgue integrable, that is,* $\int_X \| u(x) \|_{\mathcal{F}(Y)}\, dx < \infty$.

Proof. See Theorem II.2.2 of [16]. □.

Interestingly enough, we have that the set of all integrable FVMs of the form $u: X \subseteq \mathbb{R}^n \to \mathcal{F}(Y)$ forms a subspace in the vector space of measurable FVMs, which we denote by $\mathcal{M}_{\mathcal{F}}$, i.e.,

$$\mathcal{M}_{\mathcal{F}} = \{u \in (\mathcal{F}(Y))^X : u \text{is measurable}\}. \tag{12}$$

The integral of FVMs is also a linear operator from the set $\mathcal{M}_{\mathcal{F}}$ into the function space $\mathcal{F}(Y)$.

Theorem 4. *If* u *and* v *are integrable and* $\alpha, \beta \in \mathbb{R}$, *then* $\alpha u + \beta v$ *is also integrable and*

$$\int_D (\alpha u + \beta v) dx = \alpha \int_D u dx + \beta \int_D v dx \tag{13}$$

for all $D \in \Sigma$.

Proof. See Theorem 11.43 of [2]. □.

3.2. L^p spaces of FVMs

In the literature, the L^p spaces of functions that take values in a Banach space are known as *Lebesgue-Bochner* L^p *spaces* [16,45]. However, for the sake of nomenclatural simplicity, in this paper, we refer to them simply as L^p spaces. Specifically, we have the following definition.

Definition 6. Let (X, Σ, μ) be a measure space and $1 \leq p < \infty$. We define the $L^p(X; \mathcal{F}(Y))$ space as the set of all equivalence classes of μ-measurable FVMs of the form $u: X \subseteq \mathbb{R}^n \to \mathcal{F}(Y)$ such that

$$\| u \|_p := \left(\int_X \| u(x) \|_{\mathcal{F}(Y)}^p\, dx \right)^{1/p} < \infty. \tag{14}$$

In particular, if $p = \infty$, we have the space $L^{\infty}(X; \mathcal{F}(Y))$ whose elements are measurable FVMs such that

$$\| u \|_{\infty} := \operatorname*{esssup}_{x \in X} \{ \| u(x) \|_{\mathcal{F}(Y)} \} < \infty, \tag{15}$$

where the essential supremum is taken with respect to the measure μ.

Both $\|\cdot\|_{\infty}$ and $\|\cdot\|_p$ fulfill the properties of a norm, so that L^p spaces are normed spaces, which implies that $\| u \|_p$ is the norm of $u \in L^p(X; \mathcal{F}(Y))$. Moreover, if $\mathcal{F}(Y)$ is a Banach space, then $L^p(X; \mathcal{F}(Y))$ is a Banach space as well. More formally, we have the following result.

Theorem 5. *Let (X, Σ, μ) and (Y, T, ν) be finite measure spaces and let $1 \leq p \leq \infty$. If $\mathcal{F}(Y)$ is a Banach space, then $L^p(X; \mathcal{F}(Y))$ is also a Banach space.*

Proof. See Theorem 3.2.2 of [34]. □.

Given the previous theorems, it can be seen that L^p spaces of FVMs are Banach spaces. In other words, L^p spaces "inherit" the completeness of their function space $\mathcal{F}(Y)$. A similar line of arguments can be used to establish separability of L^p spaces.

Theorem 6. *If $\mathcal{F}(Y)$ is separable and $X \subset \mathbb{R}$, then $L^p(X; \mathcal{F}(Y))$ is also separable.*

Proof. See Problem 23.2 of [45], *Volume II-A*. □.

Finally, we arrive at a result that has particular importance for practical applications of the theory.

Theorem 7. *If $\mathcal{F}(Y)$ is a Hilbert space with scalar product $\langle \cdot, \cdot \rangle_{\mathcal{F}(Y)}$, then $L^2(X; \mathcal{F}(Y))$ is also a Hilbert space with scalar product defined as*

$$\langle u, v \rangle = \int_X \langle u(x), v(x) \rangle_{\mathcal{F}(Y)} dx, \tag{16}$$

for all $u, v \in L^2(X; \mathcal{F}(Y))$.

Proof. See Theorem 3.2.4 of [34]. □.

3.3. Euler-lagrange equations for FVMs

In this section, we still consider FVMs supported on a subset of $\mathbb{R}^n$, i.e., $u: X \subset \mathbb{R}^n \to \mathcal{F}(Y)$, and derive the *Euler-Lagrange equation* for functionals that take such u as their argument. In particular, we focus our attention on functionals of the following form

$$I(u) = \int_X f(x, u(x), \nabla_x u(x)) dx, \tag{17}$$

where $f: X \times \mathcal{F}(Y) \times \mathcal{G}^n(Y) \to \mathbb{R}$ is a mapping that is Fréchet differentiable with respect to all of its arguments, and $\mathcal{G}^n(Y)$ is the Cartesian product of the range of ∇_{xu}; that is, $\mathcal{G}^n(Y) = \mathcal{G}(Y) \times \cdots \times \mathcal{G}(Y)$, where $\frac{\partial u}{\partial x_i}: X \subset \mathbb{R}^n \to \mathcal{G}(Y)$. The solution of the Euler-Lagrange equation is an FVM that belongs to the set of stationary points of $I(u)$.

Theorem 8. *Let (X, Σ, μ) and (Y, T, ν) be finite measure spaces. Also, let $u: X \subseteq \mathbb{R}^n \to \mathcal{F}(Y)$, $\frac{\partial u}{\partial x_i}: X \subset \mathbb{R}^n \to \mathcal{G}(Y)$, and assume that the function*

$$\Phi(x) := f(x, u(x), \nabla_x u(x)) \tag{18}$$

is integrable over X. In addition, suppose that the Fréchet *derivatives of $f: X \times \mathcal{F}(Y) \times \mathcal{G}^n(Y) \to \mathbb{R}$ with respect to all of its arguments are continuous. Define the functional $I(u): Z(\mathcal{F}(Y), \mathcal{G}(Y)) \to \mathbb{R}$ as follows*:

$$I(u) := \int_X f(x, u(x), \nabla_x u(x)) dx, \tag{19}$$

where $Z(\mathcal{F}(Y), \mathcal{G}(Y))$ is a Banach space of FVMs that depends on the function spaces $\mathcal{F}(Y)$ and $\mathcal{G}(Y)$. If $u_0: X \subset \mathbb{R}^n \to \mathcal{F}(Y)$ is a stationary point of $I(u)$, u_0 is the solution of the equation

$$\frac{\partial f}{\partial u}(u_0) - \nabla \cdot \frac{\partial f}{\partial \nabla_x u}(\nabla_x u_0) = 0. \tag{20}$$

where $\frac{\partial f}{\partial u} \in \mathcal{F}(Y)^*$ and $\frac{\partial f}{\partial \nabla_x u} \in \mathcal{G}^n(Y)^*$ are the Fréchet *derivatives of f with respect to u and ∇_{xu} respectively, $\nabla \cdot$ is the classical divergence operator, and $\mathcal{F}(Y)^*$ and $\mathcal{G}(Y)^*$ are the dual spaces of $\mathcal{F}(Y)$ and $\mathcal{G}(Y)$ respectively.*

Proof. See Theorem 3.3.1 of [34]. □.

We consider Eq. (20) as the Euler-Lagrange equation associated with the functional $I(u)$ defined in (19). As in the case of its classical counterpart, it is a necessary condition for solutions of the variational problem stated in the previous theorem, however, it is not a sufficient condition for the existence of such solutions. To determine if such solutions exist, the standard *sufficient conditions* from calculus of variations can be employed [45].

4. Fourier transforms of FVMs

In [37], Peetre provides perhaps one of the first generalizations of the Fourier transform for Banach-valued functions. In fact, for $p \in (1, 2]$, Peetre proves that the Fourier transform is a bounded operator from $L^p(\mathbb{R}; Z)$ to $L^q(\mathbb{R}; Z)$, where q is the Hölder conjugate of p and Z is a Banach space. This result was further extended by Milman in [32], where it is proved that the Fourier transform is a well defined operator from $L^p(G; Z)$ to $L^q(\widehat{G}; Z)$, where G is a locally compact abelian group and $\widehat{G}$ its *Pontryagin dual*[1].

Based on the above results and on the definition of the Bochner integral [2], the following definition of the Fourier transform was proposed in [40],

$$U(\omega) := \int_{\mathbb{R}^n} e^{i\omega \cdot x} u(x) dx, \tag{21}$$

where $u: \mathbb{R}^n \to \mathcal{H}$ is an element of $L^1(\mathbb{R}^n; \mathcal{H})$, with $\mathcal{H}$ being a separable Hilbert space. As detailed in [40], $U(\omega)$ can be shown to be well-defined, bounded operator from $L^1(\mathbb{R}^n; \mathcal{H})$ to $L^{\infty}(\mathbb{R}^n; \mathcal{H})$. Unfortunately, no definition of the inverse Fourier transform is given in the above study.

The already existing definitions of the Fourier transforms for Banach-valued functions provide the foundation for defining the Fourier transform of FVMs. In particular, we focus our attention on the elements of the space of integrable FVMs, i.e., $L^1(\mathbb{R}^n; \mathcal{F}(Y))$.

Definition 7. Let $u \in L^1(\mathbb{R}^n; \mathcal{F}(Y))$, with the space $\mathcal{F}(Y)$ being complex-valued. We define the Fourier transform of u as the integral[2]

$$\mathbf{F}\{u\}(\omega) := U(\omega) = \int_{\mathbb{R}^n} e^{-i\omega \cdot x} u(x) dx, \tag{22}$$

where $\omega \in \mathbb{R}^n$.

Technically, ω must belong to the Pontryagin dual of $\mathbb{R}^n$. However, the Euclidean space $\mathbb{R}^n$ is a locally compact abelian group that is self-dual, and therefore ω is again an element of $\mathbb{R}^n$. Moreover, in a general setting, it is customary to employ the Haar measure when integration is carried out over a locally compact topological group. However, in the case of $\mathbb{R}^n$, the Haar measure is Lebesgue measure.

Remark 1. The Fourier transform in (22) could be viewed as a generalization of the classical definition of the Fourier transform of a vector-valued function u. Recall that in such (finite-dimensional) case, the Fourier transform of $u = (u_1, u_2, \ldots, u_m): X \subseteq \mathbb{R}^n \to \mathbb{R}^m$ is standardly obtained through transforming each component u_i of u independently. In this regard, it is interesting to observe this classical construct follows naturally from its generalization in (22) through setting $\mathcal{F}(Y) = \mathbb{R}^m$.

Theorem 9. *The Fourier transform* $\mathbf{F}$ *in (22) is a bounded operator of the form*

$$\mathbf{F}: L^1(\mathbb{R}^n; \mathcal{F}(Y)) \to L^{\infty}(\mathbb{R}^n; \mathcal{F}(Y)). \tag{23}$$

[1] In brief, the Pontryagin dual is the set of all frequencies ω. The "nature" of this dual is determined by how the set G is defined (e.g., the real line, a finite cyclic group, etc.)

[2] Note that, as opposed to (21), we define the exponential to have a negative argument, which is more conventional to image processing.

Proof. See Theorem 4.2.1 of [34]. □.

Unfortunately, the inverse transform operator is not well-defined for all elements in $L^\infty(\mathbb{R}^n; \mathcal{F}(Y))$, as not all FVMs in this space lie in $L^1(\mathbb{R}^n; \mathcal{F}(Y))$. As such, we define the inverse transform under the assumption that both u and U belong to $L^1(\mathbb{R}^n; \mathcal{F}(Y))$, as is customary in harmonic analysis [18].

Definition 8. If both u and U are elements of $L^1(\mathbb{R}^n; \mathcal{F}(Y))$, the inverse Fourier transform of U can be defined as

$$\mathbf{F}^{-1}\{U\}(\omega) := \frac{1}{(2\pi)^n}\int_{\mathbb{R}^n} e^{i\omega\cdot x}U(\omega)d\omega. \tag{24}$$

The measure of the above integral is defined as the *dual measure* $\hat{\mu}$ of μ. In our particular case, we have $\hat{\mu} = \frac{1}{(2\pi)^n}\mu$ [18].

Theorem 10. *If both u and U belong to $L^1(\mathbb{R}^n; \mathcal{F}(Y))$, then*

$$u(x) = \frac{1}{(2\pi)^n}\int_{\mathbb{R}^n} e^{i\omega\cdot x}\, U(\omega)d\omega, \tag{25}$$

where $U(\omega)$ is defined in (22).

Proof. See Theorem 4.2.2 of [34]. □.

It is clear that the operators $\mathbf{F}$ and $\mathbf{F}^{-1}$ are linear, which is, of course, a consequence of the linearity of the Bochner integral. Formally, for any $\alpha, \beta \in \mathbb{C}$ and $u, v \in L^1(\mathbb{R}^n; \mathcal{F}(Y))$ we have

$$\mathbf{F}\{\alpha u + \beta v\} = \alpha\mathbf{F}\{u\} + \beta\mathbf{F}\{v\}, \tag{26}$$

and

$$\mathbf{F}^{-1}\{\alpha U + \beta V\} = \alpha\mathbf{F}^{-1}\{U\} + \beta\mathbf{F}^{-1}\{V\}. \tag{27}$$

Moreover, as in the classical case, Fourier transforms of FVMs also possess many useful properties which relate the Fourier transform of an FVM u with that of its shifted, modulated, scaled, as well as differentiated and integrated versions, as detailed in the next two theorems.

Theorem 11. *Let $u \in L^1(\mathbb{R}^n; \mathcal{F}(Y))$ and $U(\omega)$ be its Fourier transform. Also, let $\omega_0, x_0 \in \mathbb{R}^n$ and $a \in \mathbb{R}$, $a \neq 0$. Then, the following assertions hold*

1. **Translation:** $\mathbf{F}\{u(x - x_0)\} = e^{-i\omega\cdot x_0}U(\omega)$.
2. **Modulation:** $\mathbf{F}\{e^{-i\omega_0\cdot x}u(x)\} = U(\omega - \omega_0)$.
3. **Scaling:** $\mathbf{F}\{u(ax)\} = \frac{1}{|a|^n}U(\frac{\omega}{a})$.
4. **Integration:** $\int_{\mathbb{R}^n} u(x)dx = U(0)$.

Proof. *See Theorem 4.2.3 of* [34]. □.

Theorem 12. *Assume all $\frac{\partial^l u}{\partial x_j^l}$ and $(i\omega_j)^l U$ are elements of $L^1(\mathbb{R}^n; \mathcal{F}(Y))$ with $0 \le l \le k$. Then,*

$$\mathbf{F}\left\{\frac{\partial^k u}{\partial x_j^k}\right\}(\omega) = (i\omega_j)^k U(\omega). \tag{28}$$

Proof. See Theorem 4.2.4 of [34]. □.

It is interesting to observe that, similarly to the classical case, the Fourier transform in (28) diagonalizes the differential operator. The following result shows that the diagonalization properties of the Fourier transform extend to the convolution operator as well. In fact, the theorem generalizes the famous convolution theorem for scalar- and vector-valued functions.

Theorem 13. *For $u, v \in L^1(\mathbb{R}^n; \mathcal{F}(Y))$,*

$$(u^*v)(x) := \int_{\mathbb{R}^n} u(x - z)v(z)dz = \int_{\mathbb{R}^n} u(z)v(x - z)dz \tag{29}$$

is in $L^1(\mathbb{R}^n; \mathcal{F}(Y))$ and

$$\mathbf{F}\{u^*v\} = \mathbf{F}\{u\}\mathbf{F}\{v\}. \tag{30}$$

Proof. See Theorem 4.2.5 of [34]. □.

5. Fractal transforms on FVMs and associated operators on their fourier transforms

In [42], the FVM formalism was applied to processing of hyperspectral (HS) images, which can be considered to be FVMs from a *pixel space* X to $L^2(\mathbb{R})$. The main objective of the study was to explore some basic self-similarity properties of HS images, which has led to the formulation of a family of *fractal transforms* acting upon them. A rigourous mathematical framework for such transforms was further developed in [43]. One of the main results of the above study was to show that, under certain conditions, a fractal transform T can be contractive, which implies the existence of a fixed point $\bar{u}$ such that $T\bar{u} = \bar{u}$. Naturally, this leads to the *inverse problem* of fractal image coding, which consists in finding a fractal transform T with fixed point $\bar{u}$ that approximates a given u to a sufficient degree of accuracy. As in the case with fractal coding of greyscale images, this problem can be solved by means of *collage-based coding* [25] (to be defined in Section 5.3), seeking a fractal transform T that maps the image u as close to itself as possible.

In what follows, we outline the mathematical framework for fractal transforms of FVMs. Our principal motivation is to show that a fractal transform T acting on an FVM u induces an operator T^* on the Fourier transform U of u.

5.1. A complete metric space (Z, d_Z) of hyperspectral images

In the context of HS processing, data images are interpreted as FVMs from a pixel (or base) space X to the space of *spectral functions* $\mathcal{F}(Y)$ [31,42]. More specifically, we consider the following practical settings and their related definitions.

- **The base space** X: The compact support of HS images, with metric d_X. For convenience, we assume $X = [0, 1]^n$, where n=1,2 or 3.
- **The spectral space** $\mathcal{F}(Y)$: The space $L^2(\mathbb{R}_s)$ of square-integrable functions supported on a compact set $\mathbb{R}_s \subset \mathbb{R}_+ := \{y \in \mathbb{R} | y \ge 0\}$. As follows from Theorem 7, $L^2(\mathbb{R}_s)$ is a Hilbert space with the standard definition of the inner product, i.e.,

$$\langle f, g\rangle = \int_{\mathbb{R}_s} f(y)g(y)dy, \ \forall f, g \in L^2(\mathbb{R}_s). \tag{31}$$

In what follows, the norm defined by the above inner product will be denoted by $\|\cdot\|_{L^2(\mathbb{R}_s)}$.

Now, let Z denote the set of all FVMs from X to $L^2(\mathbb{R}_s)$. Given a $u \in Z$, then at any particular $x \in X$, $u(x)$ is an element of the space $L^2(\mathbb{R}_s)$. Moreover, following [31], the norm $\|\cdot\|_{L^2(\mathbb{R}_s)}$ may be used to define a norm $\|\cdot\|_Z$ on Z which, in turn, defines a metric d_Z on Z. Specifically, for any $u, v \in Z$, we have

$$d_Z(u, v) = \left[\int_X \| u(x) - v(x)\|^2_{L^2(\mathbb{R}_s)}\, dx\right]^{1/2}. \tag{32}$$

By Theorem 5, the space $L^2(X; L^2(\mathbb{R}_s))$ is complete, which implies that the metric space (Z, d_Z) of HS images is complete as well.

5.2. A class of fractal transforms on (Z, d_Z)

We are now in position to introduce a class of fractal transforms on Z. For the sake of notational simplicity, we assume the HS images to be defined over "one-dimensional" pixel space $X = [0, 1]$. The extension to $[0, 1]^n$ (and, in particular, n=2) is straightforward. The following items will be required to formalize our results.

1. A set of N one-to-one, affine contraction mappings $w_i: X \to X$,

$w_i(x) = s_i x + a_i$, $x \in X$, with the condition that $\cup_{i=1}^{N} w_i(X) = X$. In other words, the contracted copies, or "tiles" of X, $w_i(X)$, cover X.

2. Associated with each map w_i are the following:
   (a) A scalar $\alpha_i \in \mathbb{R}$ and
   (b) A function β_i: $\mathbb{R}_s \to \mathbb{R}_+$, $\beta_i \in L^2(\mathbb{R}_s)$.

Consequently, for an arbitrary $u \in Z$ and $x \in X$, the fractal transform T: $Z \to Z$ is defined as follows,

$$v(x) = (Tu)(x) = \sum_{i=1}^{N}{}' [\alpha_i u(w_i^{-1}(x)) + \beta_i], \tag{33}$$

where the prime indicates that the summation is carried out over only those $i \in \{1, 2, \ldots, N\}$ for which the preimage $w_i^{-1}(x)$ exists, i.e., those i for which $x \in w_i(X)$.

The above formulation represents a generalization of the standard fractal transform for greyscale images [17,29]. The value of the HS image $v(x) = (Tu)(x)$ at a point $x \in X$ is a spectral function, i.e., $v(x) \in L^2(\mathbb{R}_s)$. Furthermore, the values of $v(x)$ at $y \in \mathbb{R}_s$ are given by

$$v(x)(y) = (Tu)(x)(y) = \sum_{i=1}^{N}{}' [\alpha_i u(w_i^{-1}(x))(y) + \beta_i(y)]. \tag{34}$$

The function $\beta_i(y)$ replaces the traditional constant β_i employed in standard fractal transforms for scalar-valued image functions [17,29].

The following theorem shows that the fractal transform defined in (33) can be contractive.

Theorem 14. *Given the fractal transform T defined in (33), for any $u, v \in Z$,*

$$d_Z(Tu, Tv) \le K d_Z(u, v), \tag{35}$$

where

$$K = \sum_{i=1}^{N} |s_i|^{1/2} |\alpha_i| \ge 0. \tag{36}$$

Proof. *We simply find a bound for $d_Z(Tu, Tv)$:*

$$\begin{aligned} d_Z(Tu, Tv) &= \left(\int_X \| \sum_{i=1}^{N} \alpha_i (u(w_i^{-1}(x)) - v(w_i^{-1}(x))) \|^2_{L^2(\mathbb{R}_s)} \, dx \right)^{1/2} \\ &\le \sum_{i=1}^{N} \left(\int_{w_i(X)} \| \alpha_i (u(w_i^{-1}(x)) - v(w_i^{-1}(x))) \|^2_{L^2(\mathbb{R}_s)} \, dx \right)^{1/2} \\ &= \sum_{i=1}^{N} \left(|s_i| \int_X \| \alpha_i (u(z) - v(z)) \|^2_{L^2(\mathbb{R}_s)} \, dz \right)^{1/2} \\ &= \left(\sum_{i=1}^{N} |s_i|^{1/2} |\alpha_i| \right) \left(\int_X \| u(z) - v(z) \|^2_{L^2(\mathbb{R}_s)} \, dz \right)^{1/2} = K d_Z(u, v). \end{aligned} \tag{37}$$

□

The following result is a consequence of Banach's Fixed Point Theorem.

Corollary 1. *If T is contractive on Z* (i.e., $K < 1$), *there exists a unique $\bar{u} \in Z$, the fixed point of T, such that $\bar{u} = T\bar{u}$. Furthermore, let $u_0 \in Z$ be any "seed" for the iteration sequence $u_{n+1} = Tu_n$. Then $u_n \to \bar{u}$ as $n \to \infty$,* i.e., $d_Z(u_n, \bar{u}) \to 0$.

From Eq. (34), the fixed point FVM, $\bar{u}$, of a contractive fractal transform T obeys the following "self-similarity" relation,

$$\bar{u}(x)(y) = \sum_{i=1}^{N}{}' [\alpha_i \bar{u}(w_i^{-1}(x))(y) + \beta_i(y)]. \tag{38}$$

In other words, $\bar{u}$ may be expressed as a linear combination of scaled and spatially-contracted copies of itself, along with the addition of the "shift functions" β_i.

5.3. Inverse problem for fractal transforms on (Z, d_Z)

We now consider the following inverse problem, a hyperspectral version of fractal image coding [5,17,29]: Given a target FVM $u \in Z$, find a contractive fractal transform T: $Z \to Z$, such that its fixed point $\bar{u}$ approximates u to a desired accuracy, i.e., $d_Z(\bar{u}, u)$ is sufficiently small. Given the complicated nature of the fractal transform T, such direct problems are intractable. An enormous simplification is achieved by means of the following simple consequence of Banach's Fixed Point Theorem, known in the fractal coding literature as the *Collage Theorem* [4].

Theorem 15. *If the fractal transform T in (33) is contractive on Z* (*i.e.*, $K < 1$) *with fixed point $\bar{u} \in Z$, then for any $u \in Z$,*

$$d_Z(u, \bar{u}) \le \frac{1}{1 - K} d_Z(u, Tu). \tag{39}$$

The above result is not restricted to fractal transforms – it applies in general to contraction maps T on complete metric spaces (X,d). In *collage-based coding* [25], one looks for a contractive fractal transform T that maps a target $u \in X$ as close as possible to itself, in an effort to make the so-called "collage error," $d(u, Tu)$, as small as possible.

One of the original motivations for fractal image coding was *image compression* [5,17,29]. In Section 6, we outline a simple fractal coding method for HS images. More details are to be found in [42,43].

5.4. Induced fractal operator on the space of Fourier transforms

As in the previous section, let us consider the space $Z = L^2(X; L^2(\mathbb{R}_s))$ with $X = [0, 1]$. Since X is a finite measure space, each $u \in Z$ is also an element of $L^1(X; L^2(\mathbb{R}_s))$. Consider the L^1 norm of u:

$$\| u \|_1 = \int_X \| u(x) \|_{L^2(\mathbb{R}_s)} \, dx. \tag{40}$$

By using the Hölder inequality we have that

$$\int_X \| u(x) \|_{L^2(\mathbb{R}_s)} \, dx \le \mu(X)^{\frac{1}{2}} \left(\int_X \| u(x) \|^2_{L^2(\mathbb{R}_s)} \, dx \right)^{\frac{1}{2}} \tag{41}$$

$$= \left(\int_X \| u(x) \|^2_{L^2(\mathbb{R}_s)} \, dx \right)^{\frac{1}{2}} \tag{42}$$

$$= \| u \|_Z. \tag{43}$$

Thus, it is possible to calculate the Fourier transform of u which is also an FVM,

$$U(\omega) = \mathbf{F}\{u\}(\omega) = \int_X e^{-i\omega x} u(x) dx, \quad \omega \in \mathbb{R}. \tag{44}$$

Consequently, one can define the following space,

$$\begin{aligned} \mathfrak{F}(Z) = \{ U = \mathbf{F}\{u\}, u \in L^1(X; L^2(\mathbb{R}_s)) : U \in L^\infty(\mathbb{R}^n; L^2(\mathbb{R}_s)) \\ \cap L^1(\mathbb{R}^n; L^2(\mathbb{R}_s)) \}. \end{aligned} \tag{45}$$

Theorem 16. *$\mathfrak{F}(Z)$ is a closed subset of $L^\infty(\mathbb{R}^n; L^2(\mathbb{R}_s))$ and complete with respect to the $\|\cdot\|_\infty$ norm.*

Proof. *Let $U_n \in \mathfrak{F}(Z)$ be a convergent sequence of Fourier transforms to $U \in L^\infty(\mathbb{R}^n; L^2(\mathbb{R}_s))$. We aim at showing that $U \in \mathfrak{F}(Z)$. Let $u_n \in Z$ be such that $U_n = \mathbf{F}\{u_n\}$: Thanks to Theorem 10, we also have that*

$$u_n(x) = \frac{1}{(2\pi)^n} \int_{\mathbb{R}^n} e^{i\omega \cdot x} U_n(\omega) d\omega, \tag{46}$$

which easily implies that u_n is a Cauchy sequence in $Z = L^2(X; L^2(\mathbb{R}_s))$ (because $X = [0, 1]$). As Z is complete, there exists a $u \in Z$ such that $u_n \to u$ when $n \to \infty$. Let $U = \mathbf{F}\{u\}$. The desired result follows from the

following simple calculation,

$$\| U - U_n \|_\infty = \operatorname*{ess\,sup}_{\omega\in\mathbb{R}} \left\{ \| \int_X e^{-i\omega x}(u_n(x) - u(x))dx \|_{L^2(\mathbb{R}_s)} \right\} \tag{47}$$

$$\leq \int_X \| u_n(x) - u(x)) \|_{L^2(\mathbb{R}_s)}\, dx \tag{48}$$

$$\leq \| u_n - u \|_Z . \tag{49}$$

Since $\| u_n - u \|_Z \to 0$, *it immediately follows that* $\| U - U_n \|_\infty \to 0$ *as well.* □

Now recall the fractal transform $T: Z \to Z$ as defined in (33). We compute the Fourier transforms of both sides of (33) in order to determine the induced fractal transform operator T^* on the space of Fourier transforms $\mathfrak{F}(Z)$:

$$\begin{aligned} W(\omega) := (T^*U)(\omega) &= \sum_{i=1}^{N}{}' \int_X e^{-i\omega x}\alpha_i u(w_i^{-1}(x))dx + \int_X e^{-i\omega x}\beta_i dx \\ &= \sum_{i=1}^{N} \alpha_i s_i \int_X e^{-i\omega(s_i y + a_i)} u(x)dx + \int_X e^{-i\omega x}\beta_i dx \\ &= \sum_{i=1}^{N} \alpha_i s_i e^{-ia_i\omega} U(s_i\omega) + \beta_i K(\omega), \end{aligned} \tag{50}$$

where

$$K(\omega) = \int_X e^{-i\omega x} dx. \tag{51}$$

The following result shows that T^* is Lipschitz continuous on $\mathfrak{F}(Z)$.

Theorem 17. *The fractal operator* $T^*: \mathfrak{F}(Z) \to \mathfrak{F}(Z)$, *defined by* (50) *satisfies*

$$\| T^*U_1 - T^*U_2 \|_\infty \leq K^* \| U_1 - U_2 \|_\infty \tag{52}$$

where

$$K^* = \sum_{i=1}^{N} |\alpha_i| |s_i|. \tag{53}$$

Proof.

$$\begin{aligned} \| T^*U_1 - T^*U_2 \|_\infty &\leq \sum_{i=1}^{N} |\alpha_i s_i e^{-ia_i\omega}| \operatorname*{ess\,sup}_{\omega\in\mathbb{R}} \{ \| U_1(s_i\omega) - U_2(s_i\omega) \|_{L^2(\mathbb{R}_s)} \} \\ &\leq \sum_{i=1}^{N} |\alpha_i| |s_i| \| U_1 - U_2 \|_\infty = K^* \| U_1 - U_2 \|_\infty . \end{aligned} \tag{54}$$

□

Corollary 2. *If* T^* *is contractive on* $\mathfrak{F}(Z)$ (*which is guaranteed if* $K^* < 1$),*then there exists a unique* $\overline{U} \in \mathfrak{F}(Z)$, *the fixed point of* T^*, *such that* $\overline{U} = T^*\overline{U}$. *Furthermore, let* $U_0 \in \mathfrak{F}(Z)$ *be any* "seed" *for the iteration sequence* $U_{n+1} = T^*U_n$. *Then* $U_n \to \overline{U}$ *as* $n \to \infty$, i.e., $\| U_n - \overline{U} \|_\infty \to 0$.

From (50), the fixed point Fourier transform, $\overline{U}$, of a contractive fractal transform operator T^* obeys the following "self-similarity" relation,

$$\overline{U}(\omega) = \sum_{i=1}^{N} \alpha_i s_i e^{-ia_i\omega} \overline{U}(s_i\omega) + \beta_i K(\omega). \tag{55}$$

In other words, $\overline{U}$ may be expressed as a linear combination of scaled, phase-shifted and *frequency-contracted* copies of itself, along with the addition of the modified "shift functions," $\beta_i K(\omega)$. The fact that the copies are contracted in frequency space is a consequence of the complimentarity of space (or time) and frequency domains. A similar complimentarity in the self-similarity relations for fixed points of fractal transforms and their Fourier transforms in the classical, scalar-valued case was derived and exploited in [30].

In closing this section, we mention that the idea of a fractal transform inducing a corresponding transform on a "dual" transform space is not new. Perhaps one of the earliest systematic treatments, for the case of orthogonal expansions of scalar-valued functions, including wavelet expansions, is to be found in [19]. A discussion of transforms induced by fractal transforms on both function as well as measure spaces is given in [25].

6. Applications

In this section, we present two applications that employ the FVM formalism, namely, denoising (using the Euler-Lagrange method of Section 3.3) and fractal coding of HS images. Of course, any practical application of our formalism will involve the processing of *digital* HS images supported on an $N_1 \times N_2$-pixel array, M channels per pixel. As such, a digital HS image is a "data cube" which can be represented by a vector-valued image function $u: X \to \mathbb{R}^M$, where $X = \{1, 2, \ldots, N_1\} \times \{1, 2, \ldots, N_2\}$ is the *base* or *pixel space* and $\mathbb{R}_+^M$, the nonnegative orthant of $\mathbb{R}^M$, is the *spectral space*. At a pixel location $(i_1, i_2) \in X$, the digital HS image function $u(i_1, i_2)$ is a non-negative M-vector with components $u_k(i_1, i_2)$, $1 \leq k \leq M$. We shall refer to this vector as the *spectral function* at pixel (i_1, i_2).

6.1. A simple denoising scheme

If HS images are represented as FVMs there are several ways in which the inverse problem of denoising can be addressed. In this section we describe one possible method which employs a very simple denoising model. We begin with the assumption that the HS images in which we are interested belong to $C^2(X; L^2(Y))$, where X and Y are subsets of $\mathbb{R}^2$ and $\mathbb{R}$ respectively. Admittedly, this is a quite strong requirement on the HS image in the spatial direction—piecewise $C^2(X; L^2(Y))$ would be more "realistic". Our assumption allows us to use the previous formulation of the Euler-Lagrange equation, where all derivatives are understood to be in the classical sense, along with our definition of Fourier transforms for FVMs to arrive at a simple denoising method.

That being said, our regularity assumption can be weakened by introducing the notion of the variational derivative which, in turn, requires the use of the weak formulation of the Euler-Lagrange equation, where all derivatives are defined in the weak sense. In this way, we could assume, more realistically, that the HS images are piecewise continuous or perhaps even functions of bounded variation. This, however, is beyond the scope of this paper and will be addressed elsewhere.

With this regularity assumption in mind, we seek to recover a denoised reconstruction $\overline{u}$ of an HS image from a noisy observation f by minimizing the following functional, $I: C^2(X; L^2(Y)) \to \mathbb{R}$:

$$\min_u \left\{ \frac{1}{2} \| \rho(u - f) \|_2^2 + \int_X \| \nabla_x u(x) \|_2^2 \, dx \right\}. \tag{56}$$

Here we acknowledge that the L^2-squared norm of the gradient—a kind of "elastic bending" term—is not an optimal norm in terms of denoising ability—an L^1 norm of the gradient (total variation) would be more effective. The L^2-squared norm was chosen because it yields a closed-form solution in terms of Fourier transforms.

Also note that we allow the regularization parameter $\rho = \rho(y)$ to be a function of the spectral parameter $y \in Y$, representing the possibility of imposing different strengths of the denoising process throughout the spectral space Y.

From Section 3.3, the Euler-Lagrange equation which corresponds to Eq. (56) is given by

$$\int_Y \left[\rho(u(x) - f(x))(y) - \left(\frac{\partial^2 u(x)}{\partial x_1^2} - \frac{\partial^2 u(x)}{\partial x_2^2} \right)(y) \right] dy = 0, \tag{57}$$

As mentioned in Section 3.3, a solution to (57) is a stationary point of the functional $I(u)$ being minimized in (56). Here we consider the particular solution $u\colon X \to L^2(Y)$ which satisfies the following PDE,

$$\left(\frac{\partial^2 u(x)}{\partial x_1^2} + \frac{\partial^2 u(x)}{\partial x_2^2}\right)(y) - \rho(u(x) - f(x)(y) = 0, \tag{58}$$

for almost all $x \in X$ and almost all $y \in Y$ (Lebesgue measure in both cases). In this case u can be determined using the Fourier transform for FVMs. The result is the following low-pass filter,

$$u(y) = \mathbf{F}^{-1}\left\{\left[\frac{\rho(y)}{\| \omega \|_2^2 + \rho(y)}\right]\mathbf{F}\{f\}(\omega)\right\}. \tag{59}$$

Once again, the variability of the regularization parameter $\rho(y)$ can produce different degrees of denoising over the spectral space Y. In the special case that $\rho(y) = \rho_0$, a constant, we have the classical result,

$$u(y) = \mathbf{F}^{-1}\left\{\left[\frac{\rho_0}{\| \omega \|_2^2 + \rho_0}\right]\mathbf{F}\{f\}(\omega)\right\}. \tag{60}$$

Because of the simplicity of the model in (56), where there is no coupling between spectral components with different y-values, the filtering in both (59) and (60) may be performed on each y-value independently.

One final comment: Notice that when ρ is constant over Y, the average of u with respect to y is invariant across all solutions to the Euler-Lagrange Eq. (57). To see this, define the following real-valued average functions,

$$\overline{u}(x) = \int_Y u(x)(y)dy, \overline{f}(x) = \int_Y f(x)(y)dy. \tag{61}$$

From Eq. (57) one easily obtains the following PDE in $\overline{u}(x)$,

$$\frac{\partial^2 \overline{u}(x)}{\partial x_1^2} + \frac{\partial^2 \overline{u}(x)}{\partial x_2^2} - \rho(\overline{u}(x) - \overline{f}(x)) = 0 \tag{62}$$

for a.e. $x \in X$. Using the classical Fourier transform for functions, we easily obtain its solution,

$$\overline{u} = \mathbf{F}^{-1}\left\{\frac{\rho\overline{F}(\omega)}{\| \omega \|_2^2 + \rho}\right\}. \tag{63}$$

where $\overline{F}$ is the classical Fourier transform of the function $\overline{f}$.

In what follows, we present some results obtained from the denoising of two standard digital HS images, *Indian Pines* and *Salinas-A*—the latter being a subset of the *Salinas* image. Both of these images can be downloaded from [20]. The dimensions of the 3D *Indian Pines* and *Salinas-A* images, assumed to be the noiseless data sets, $N_1 \times N_2 \times M = 145 \times 145 \times 220$ and $83 \times 86 \times 224$, respectively. Additive White Gaussian Noise with constant power over all channels was added to these two data sets. In all experiments, the PSNR between the noisy and noiseless HS images was 30.103 dB.

The HS images were denoised using discrete versions of both Eqs. (59) and (60) involving the Fast Fourier Transform. For the method rendered by Eq. (59), discrete approximations, ρ_k, of $\rho(y)$, for $1 \le k \le M$, were determined experimentally by minimizing the mean squared error (MSE) between the kth channels of the denoised result u and the noiseless HS image u_0. In the case $\rho(y) = \rho_0$ (see Eq. (60)), the parameter ρ_0 was determined in the same manner.

The Peak Signal-to-Noise Ratio (PSNR) and the Structural Similarity Index Measure (SSIM) [44] were employed as measures of performance. The SSIM was computed between the original and recovered HS images in both the spatial and spectral domains. As the name suggests, the "spectral SSIM" was computed between (denoised and original) spectra. The "spatial SSIM" was computed between (denoised and original) channels. In each case, as is normally done, an overall spectral or spatial SSIM was obtained by averaging over all computed SSIMs. A summary of these results is shown in Table 1.

Table 1
Numerical results with respect to different measures of performance. The PSNR prior to denoising was 30.103 dB. The results presented in the second column correspond to the cases in which the regularizing parameter is constant. The results presented in the third column show how the denoising improves when the strength of the denoising process changes across the spectral domain.

	ρ_0	$\rho(y)$
SALINAS-A		
PSNR (dB)	33.1069	36.3229
SPATIAL SSIM	0.9008	0.9311
SPECTRAL SSIM	0.9872	0.9927
INDIAN PINES		
PSNR (dB)	31.5657	34.4031
SPATIAL SSIM	0.7368	0.8906
SPECTRAL SSIM	0.9873	0.9934

Some visual results are presented in Figs. 1 and 2. In Fig. 1 is shown the denoising result for a particular channel (No. 23) of the *Salinas* image. The noisy HS image is at the top left, the original noiseless image is at the bottom left. The denoised channel is shown at bottom right. At top right is shown the Structural Similarity (SSIM) map between the denoised and noiseless image: The brighter a given location, the greater the similarity between the denoised and original bands at that location. In Fig. 2, the denoising of a particular spectral function of the *Salinas image* (at a particular pixel) is shown.

Visual results for a channel of the *Indian Pines* HS image are shown in Figs. 3 and 4.

In closing this section, we mention that the roles of the domains X and Y in HS images—cf. Eq. (1) in the Introduction—can easily be reversed, so that X is now the spectral domain and Y is the spatial domain. In this case, where

$$u\colon X \subset \mathbb{R} \to L^2(Y),\ Y \subset \mathbb{R}^2 \tag{64}$$

associated with each spectral value $x \in X$, there is a 2D (spatial) image $u(x)$. Because of the greater regularity that HS images tend to exhibit in the spectral direction, the choice of the representation space $C^2(X; L^2(Y))$ may seem to be a more reasonable. We have shown elsewhere that, indeed, better denoising is achieved [35].

6.2. Fractal coding of HS images

Most, if not all, fractal image coding methods employ *block-based* transforms, where greyscale values supported on subblocks of an image are mapped onto modified greyscale values supported on smaller subblocks of the image, following the original method of Jacquin [23]. We shall employ basically the same strategy for HS images. It is tempting to perform fractal image coding on each channel of an HS image separately. This, however, is contrary to the spirit of function-valued mappings. The simple block-based fractal transform described below operates on entire spectral functions.

As done in [1] for greyscale images, we let $\mathcal{R}^{(n)}$ denote a set of $N_\mathcal{R}$ nonoverlapping $n \times n$-pixel *range* subblocks $R_i \subset X$ such that $X = \cup_i R_i$, i.e., $\mathcal{R}^{(n)}$ forms a partition of the pixel space X. Furthermore, let $u(R_i)$ denote the portion of the digital HS image function u that is supported on subblock R_i. In addition, let $\mathcal{D}^{(m)}$ denote a set of $N_\mathcal{D}$ $m \times m$-pixel *domain* subblocks $D_j \subset X$ where, for simplicity, $m = 2n$. This set need not be overlapping but the blocks should cover X, i.e., $\cup_{j=1} D_j = X$.

Given an M-channel digital HS image u, the fractal transform operator T is constructed as follows: For each image subblock $R_i \in \mathcal{R}^{(n)}$, we choose from $\mathcal{D}^{(m)}$ a domain block $u(D_{j(i)})$ in order to produce an approximation of the form

$$u(R_i) \cong (Tu)(R_i) = \alpha_i u(\widehat{D_{j(i)}}) + \underline{\beta}_i,\ 1 \le i \le N_\mathcal{R}. \tag{65}$$

Here $\underline{\beta}_i = (\beta_{i1}, \beta_{i2}, \ldots, \beta_{iM})$ is an M-vector which plays the role of the $\beta_i(t)$

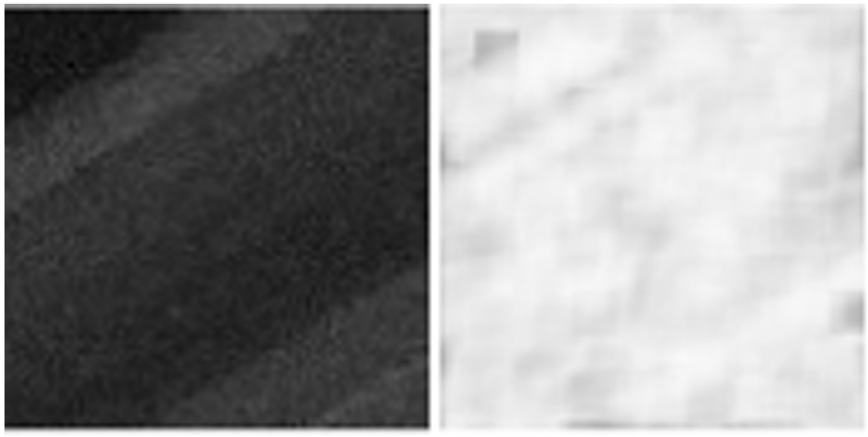

Left: Noisy band. Right: SSIM map.

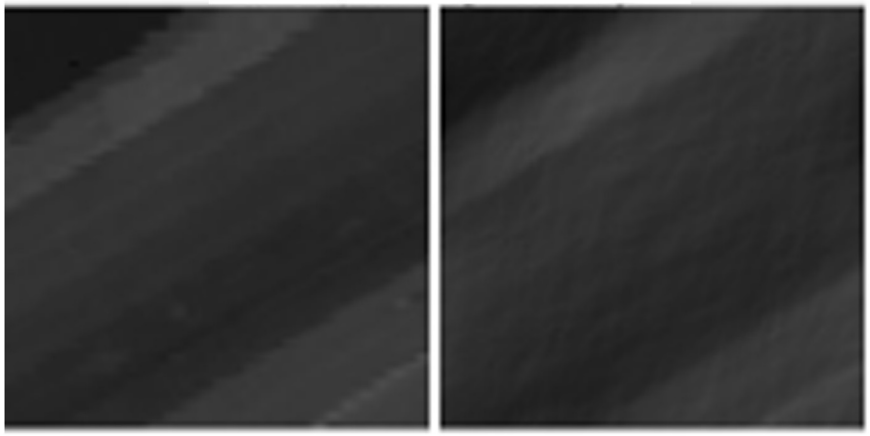

Left: Original band Right: Recovered band.

Fig. 1. Visual results for band No. 23 of the *Salinas* HS image.

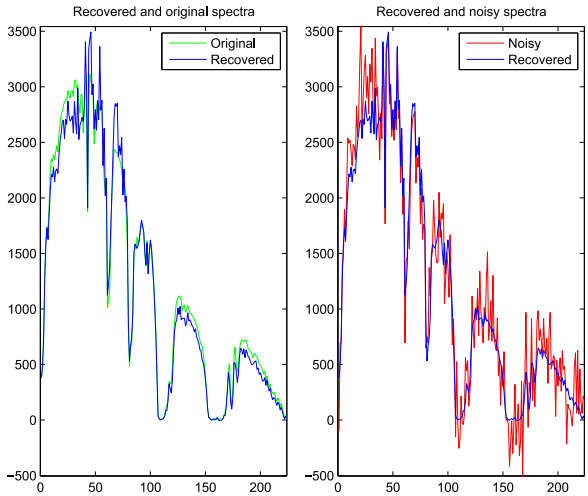

Fig. 2. Denoising results for a particular spectral function of the *Salinas* HS image. For the purpose of comparison, the original spectrum (green plot) along with the corresponding reconstruction (blue plot) can be observed in the figure at the left. The reconstruction (blue plot) and noisy spectrum (red plot) are shown in the figure at the right.

function in Eq. (33). The term $\widehat{D_{j(i)}}$ denotes an appropriate $2n \times 2n \to n \times n$-pixel decimation operation which produces the geometric contraction in discrete pixel space. Note that only **one** constant α_i is employed for all M channels supported on range block R_i—the M channels are not coded separately.

The approximation problem in Eq. (65) may be expressed in the general form,

$$y_{lm} \cong \alpha x_{lm} + \beta_m,\ 1 \le l \le N,\ 1 \le m \le M, \tag{66}$$

where $N = N_1 \times N_2$. For simplicity, the $N_1 \times N_2$ matrices in pixel space have been converted into Q-vectors. The "stack" of M N-vectors y_{lm} contain the elements of the range block $u(R_i)$ being approximated. The "stack" of M N-vectors x_{lm} contain the elements of the decimated domain block $u(\widehat{D_{j(i)}})$.

The parameters α and $\beta_m, 1 \le m \le M$, which minimize the squared L^2 distance,

$$\Delta^2 = \sum_{l=1}^{N}\sum_{m=1}^{M}(y_{lm} - \alpha x_{lm} - \beta_m)^2, \tag{67}$$

are given by (details in [42])

$$\alpha = \left[\sum_{m=1}^{M}\sum_{l=1}^{N} x_{lm}(y_{lm} - \overline{y}_m)\right]\left[\sum_{l=1}^{N}\sum_{m=1}^{M} x_{lm}^2 - N\sum_{m=1}^{M}\overline{x}_m^2\right]^{-1} \tag{68}$$

and

$$\beta_m = \overline{y}_m - \alpha\overline{x}_m,\ 1 \le m \le M. \tag{69}$$

Here,

$$\overline{x}_m = \frac{1}{N}\sum_{l=1}^{N} x_{lm} \quad \text{and} \quad \overline{y}_m = \frac{1}{N}\sum_{l=1}^{N} x_{lm} \tag{70}$$

denote the (spatial) mean values on each channel.

The set of range-domain assignments, $(i, j(i))$ and spectral map parameters $(\alpha_i, \beta_{i1}, \beta_{i2}, \ldots, \beta_{iM})$ for $1 \le i \le N_R$ comprise the *fractal code* of u which defines a (block) fractal transform T. If T is contractive, then

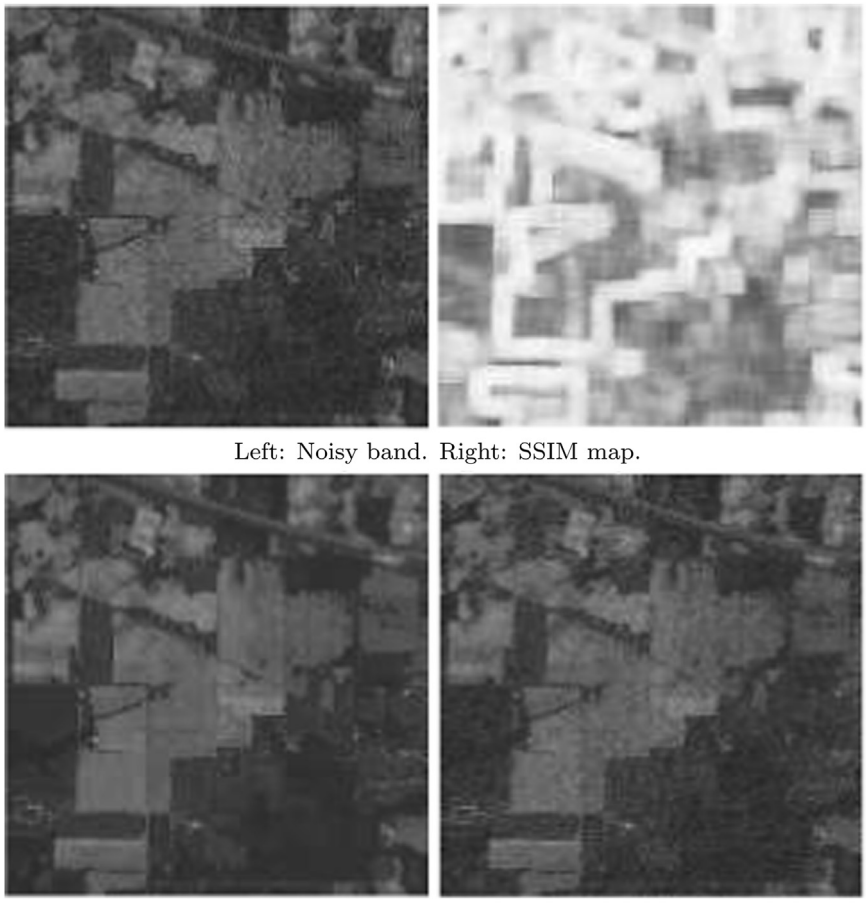

Fig. 3. Visual results for band No. 33 of the *Indian Pines* HS image.

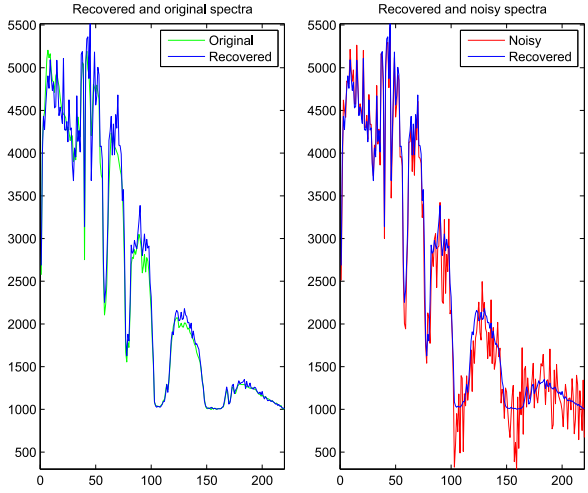

Fig. 4. Denoising results for a particular spectral function of the *Indian Pines* HS image. For the purpose of comparison, the original spectrum (green plot) along with the corresponding reconstruction (blue plot) can be observed in the figure at the left. The reconstruction (blue plot) and noisy spectrum (red plot) are shown in the figure at the right.

its fixed point HS image $\bar{u}$ may be computed by the iteration procedure $u_{n+1} = Tu_n$, where u_0 is any "seed" HS image, e.g., $u_0 = \mathbf{0}$.

It now remains to find the "best" fractal transform T associated with a given HS image u, i.e., the transform T with fixed point $\bar{u}$ that approximates u as best as possible. Because the range blocks R_i are nonoverlapping, the sums of the errors associated with the approximations in Eq. (65) defines the total collage error $d_Z(u, Tu)$ on the right hand side of Eq. (39). Since our goal is to make the approximation error $d_Z(u, \bar{u})$ on the left hand side of Eq. (39) as small as possible, we choose, for each image range block $u(R_i)$, the image domain block $u(D_{j(i)})$ which *best approximates* $u(R_i)$, i.e., which minimizes the (squared) error in Eq. (67). If we let Δ_{ik} denote the error in approximating a range block $u(R_i)$ with a domain block $u(D_k)$ (after decimation), i.e.,

$$\Delta_{ik} = \min_{\alpha,\underline{\beta}} \| u(R_i) - \alpha u(\widehat{D_k}) - \underline{\beta} \|_2, \tag{71}$$

then the index $j(i)$ of the optimal domain block $u(D_{j(i)})$ associated with $u(R_i)$ is

$$j(i) = \arg \min_k \Delta_{ik}. \tag{72}$$

We now show some results of our rather simple block-based fractal transform as applied to the AVIRIS (Airborne Visible/Infrared Imaging Spectrometer) image, "Yellowstone calibrated scene 0″, a 512 line, 677 samples per line, 224-channel image, available from [3]. The computations reported below were performed on a 512×512-pixel section of this image. The range blocks R_i used were $N_{\mathcal{R}} = 4096$ nonoverlapping 8×8-pixel blocks. The domain blocks D_i were $N_{\mathcal{D}} = 1048$ nonoverlapping 16×16-pixel blocks.

In Fig. 5 are shown some results of this fractal coding procedure: Channels 20, 120 and 220 of the original AVIRIS image on the left along with the corresponding channels of the fixed point approximation $\bar{u}$ on the right. After the fractal code of the AVIRIS image was obtained, the fixed point $\bar{u}$ was generated using the iteration procedure $u_{n+1} = Tu_n$ starting with the zero image $u_0 = \mathbf{0}$. Reasonable convergence of the procedure was obtained at u_{20}.

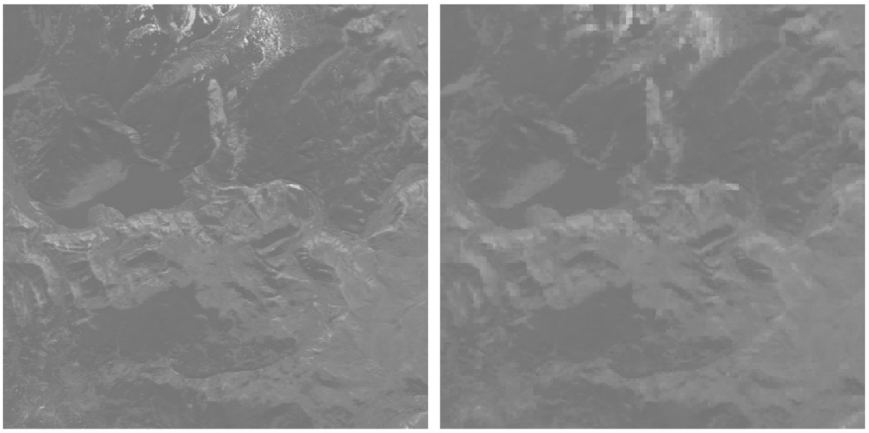

Channel 20. Left: Original. Right: Fractal-based approximation.

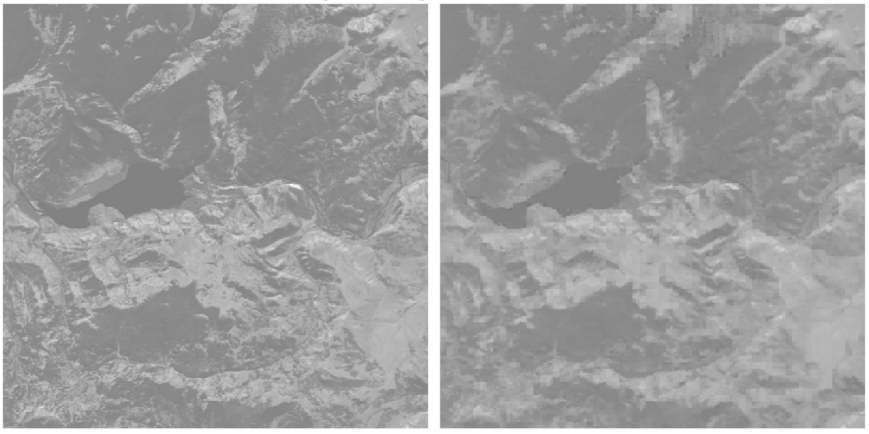

Channel 120. Left: Original. Right: Fractal-based approximation.

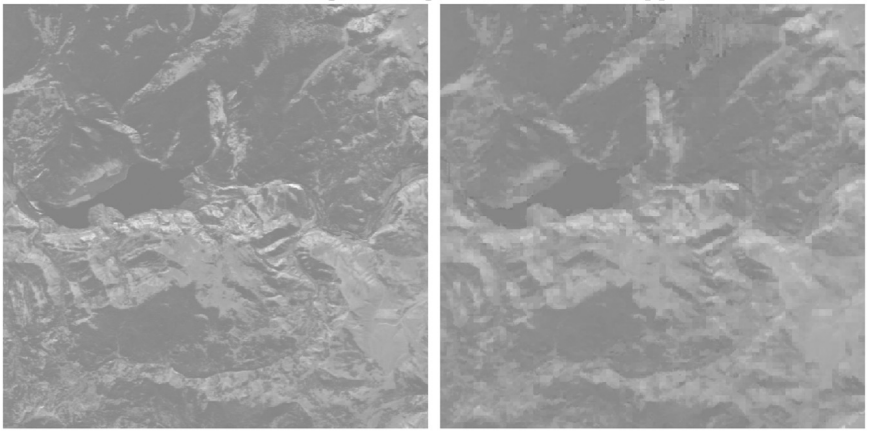

Channel 220. Left: Original. Right: Fractal-based approximation.

Fig. 5. Some channels of the attractor $\bar{u}$ of the fractal transform T obtained by fractally coding the AVIRIS hyperspectral image using 8×8-pixel range blocks and 16×16-domain blocks.

7. Final remarks

We have established a connection between the mathematical theory of FVMs and image processing, showing that is possible to carry out image processing tasks without relying on the classical finite-dimensional vector-valued approach. Some simple imaging tools were presented and applied in an application where high dimensionality is always present, namely, hyperspectral images.

On the other hand, we have employed only part of the large amount of available mathematical theory of Banach-valued functions. In the future, we plan to continue our investigation of ways in which existing mathematical results on Banach-valued functions can be applied to image processing. For example, in [33,38], formulations of total variation for Banach-valued functions are provided. To the best of our knowledge, however, these contributions have not yet been employed in imaging. Also, the concept of *sparsity* has not yet been explored in the FVM context, which could provide new state-of-the-art algorithms for imaging applications.

Lastly, it is worthwhile to mention that we have considered only FVMs whose range is a space of either real- or complex-valued functions. It would also be interesting to explore the notion of vector-FVMs, that is, FVMs whose range is a vector-valued Banach space. In this case, u: $X \subseteq A \to \mathcal{F}^n(Y)$:

$$u(x) = [u_1(x), \ldots, u_n(x)]^T. \tag{73}$$

Observe that each u_i, $1 \leq i \leq n$, is a FVM of the form u_i: $X \subset A \to \mathcal{F}(Y)$.

The importance of this representation is that it allows to parallelize image processing tasks. For instance, if each u_i is a HS image, a set of n HS datasets can be, say, denoised at the same time with a denoising algorithm that is based on this representation.

Acknowledgements

This work has been supported in part by Discovery Grants (ERV and OM) from the Natural Sciences and Engineering Research Council of Canada (NSERC Grant No. ERV 106270-2012). Financial support from the Faculty of Mathematics and Department of Applied Mathematics, University of Waterloo (DO) is also gratefully acknowledged.

References

[1] S.K. Alexander, E.R. Vrscay, S. Tsurumi, A simple, general model for the affine self-similarity of images, in: Proceedings of the International Conference on Image Analysis and Recognition, Springer, 2008, pp. 192–203.
[2] C.D. Aliprantis, K.C. Border, Infinite Dimensional Analysis: a Hitchhiker's Guide, Springer, 2006.
[3] AVIRIS hyperspectral image, Yellowstone Calibrated Scene 0, available from Information Processing Group website, Jet Propulsion Laboratory, California Institute of Technology, ⟨http://compression.jpl.nasa.gov/hyperspectral/⟩
[4] M.F. Barnsley, Fractals Everywhere, Academic Press, New York, 1988.
[5] M.F. Barnsley, L.P. Hurd, Fractal Image Compression, AK Peters Ldt., 1993.
[6] S. Bochner, Integration von funktionen, deren werte die elemente eines vektor-raumes sind, Fundam. Math. 1 (1933) 176–262.
[7] X. Bresson, T.F. Chan, T.F., Fast dual minimization of the vectorial total variation norm and applications to color image processing, Inverse Problems and Imaging, 2, 2008, pp. 455–484.
[8] A. Buades, B. Coll, J-M. Morel, A non-local algorithm for image denoising, in: Proceedings of the Conference on Computer Vision and Pattern Recognition, IEEE, 2005, pp. 60–65.
[9] A. Buades, B. Coll, J.-M. Morel, A review of image denoising algorithms with a new one, SIAM Multiscale Model. Simul. 4 (2005) 490–530.
[10] H. Cartan, H.P. Cartan, Differential Calculus, Hermann, 1971.
[11] A. Chambolle, An algorithm for total variation minimization and applications, J. Math. Imaging Vis. 20 (2004) 89–97.
[12] A. Chakrabarti, T. Zickler, Statistics of real-world hyperspectral images, Proc. CVPR (2011).
[13] G. Chen, S.E. Qian, Denoising of Hyperspectral Imagery Using Principal Component Analysis and Wavelet Shrinkage, IEEE Trans. Geosci. Remote Sens. 49, 2011, pp. 973–980.
[14] A. de Korvin, C.E. Roberts, Interchange of vector valued integrals when the measures are bochner or pettis indefinite integrals, Bull. Aust. Math. Soc. 20 (1979) 199–206.
[15] H. Deborah, N. Richard, J.Y. Hardeberg, A comprehensive evaluation of spectral distance functions and metrics for hyperspectral image processing, IEE Sel. Top. Appl. Earth Obs. Rem. Sens. 8 (6) (2015) 3224–3234.
[16] J. Diestel, J.J. Uhl, Vector Measures, American Mathematical Society, Providence, RI, 1977.
[17] Y. Fisher (Ed.), Fractal Image Compression: Theory and Application, Springer-Verlag, New York 1995.
[18] G.B. Folland, A Course in Abstract Harmonic Analysis, CRC Press, 1995.
[19] B. Forte, E.R. Vrscay, Inverse problem methods for generalized fractal transforms, in: Fractal Image Coding and Analysis, Y. Fisher (Ed.), Volume 159 of NATO ASI Series F, Springer-Verlag, Berlin, 1998.
[20] Grupo de Inteligencia Computacional de la Universidad del País Vasco, Hyperspectral Remote Sensing Scenes, ⟨http://www.ehu.eus/ccwintco/index.php⟩.
[21] B. Goldlücke, E. Strekalovskiy, D. Cremers, The natural vectorial total variation which arises from geometric measure theory, SIAM J. Imaging Sci. 5 (2012) 537–563.
[22] J. Martín-Herrero, Anisotropic diffusion in the hypercube, IEEE Trans. Geosci. Remote Sens. 45 (2007) 1386–1398.
[23] A.E. Jacquin, Image coding based on a fractal theory of iterated contractive image transformations, IEEE Trans. Image Process., Image Process. 1 (1992) 18–30.
[24] A.K. Jain, An Introduction to Digital Image Processing.
[25] H. Kunze, D. La Torre, F. Mendivil, E.R. Vrscay, Fractal-based Methods in Analysis, Springer Science & Business Media, 2011.
[26] D. La Torre, E.R. Vrscay, M. Ebrahimi, M.F. Barnsley, Measure-valued images, associated fractal transforms, and the affine self-similarity of images, SIAM J. Imaging Sci. 2 (2009) 470–507.
[27] S. Lansell, M. Parmar, B.A. Wandell, Dictionaries for sparse representation and recovery of reflectances, in Computational Imaging VII, edited by C.A. Bouman, E. L. Miller, I. Pollak, Proceedings SPIE 7246 (2009) http://dx.doi.org/10.1117/12.813769.
[28] F. Lenti, F. Nunziata, C. Estatico, M. Migliaccio, On the spatial resolution enhancement of microwave radiometer data in banach spaces, IEEE Trans. Geo. Rem. Sens. 52 (3) (2014) 1834–1842.
[29] N. Lu, Fractal Imaging, Morgan Kaufmann Publishers Inc., 1997.
[30] G.S. Mayer E.R. Vrscay, Iterated Fourier transform systems: a method for frequency extrapolation, in: Proceedings of the International Conference on Image Analysis and Recognition, Springer, 2007, pp. 728–739.
[31] O. Michailovich, D. La Torre, E.R. Vrscay, Function-Valued Mappings, Total Variation and Compressed Sensing for diffusion MRI, in: Proceedings of the International Conference on Image Analysis and Recognition, Springer, 2012, pp. 286–295.
[32] M. Milman, Complex interpolation and geometry of banach spaces, Ann. Mat. Pura Ed. Appl. 136 (1984) 317–328.
[33] M. Miranda, Functions of bounded variation on "good" metric spaces, J. mathématiques pures appliquées 82 (2003) 975–1004.
[34] D. Otero, Function-valued Mappings and SSIM-based Optimization in Imaging, (Ph.D. thesis), University of Waterloo, Waterloo, ON, Canada, 2015.
[35] D. Otero, D. La Torre, E.R. Vrscay, Image Denoising forFunction-valued Mappings, preprint, 2016.
[36] J.P.S. Parkkinen, J. Hallikainen, T. Jaaskelainen, Characteristic spectra of munsell colors, J. Opt. Soc. Am. A 6 (2) (1989) 318–322.
[37] J. Peetre, Sur la transformation de fourier des fonctions à valeurs vectorielles, Rendicoti Del. Semin. Mat. della Univ. Padova 42 (1969) 15–26.
[38] V. Recupero, BV solutions of rate independent variational inequalities, Ann. della Sc. Norm. Super. isa-Cl. Sci.-Ser. V. 10 (2011) 269.
[39] D. Schiavulli, F. Lenti, F. Nunziata, G. Pugliano, M. Migliaccio, Landweber method in hilbert and banach spaces to reconstruct the NRCS field from GNSS-R measurements, Int. J. Rem. Sens. 35 (2014) 3782–3796.
[40] H. Thompson, The Bochner Integral and An Application to Singular Integrals, M. Sc. thesis, Dalhousie University, Halifax, NS, Canada, 2014.
[41] M. Tubaishat S.K. Madria, Sensor networks: an overview, in: Proceedings of IEEE Potentials, 22 (2), 20–23, April 2003.
[42] E.R. Vrscay, D. Otero, D. La Torre, Hyperspectral images as function-valued mappings, their self-similarity and a class of fractal transforms, in: Proceedings of the International Conference on Image Analysis and Recognition, Springer, 2013, pp. 225–234.
[43] E.R. Vrscay, D. Otero, D.La. Torre, A simple class of fractal transforms for hyperspectral images, Appl. Math. Comput. 231 (2014) 435–444.
[44] Z. Wang, A.C. Bovik, H.R. Sheikh, E.P. Simoncelli, Image quality assessment: from error visibility to structural similarity, IEEE Trans. Image Process. 13 (2004) 600–612.
[45] E. Zeidler, Nonlinear Functional Analysis and its Applications, Springer-Verlag, New York, NY, 1990.